Influence of spin-coating rotation speed and spin-coating time on $CsPbIBr_2$ perovskite thin films

FEI ZHAO[1,*], YIXIN GUO[2,*], PEIZHI YANG[3]
[1]*School of Photoelectric Engineering, Changzhou Institute of Technology, Changzhou 213032, China*
[2]*Department of Physics, Shanghai Normal University, Shanghai 200233, China*
[3]*College of Energy and Environmental Science, Yunnan Normal University, Kunming 650500, China*

All-inorganic $CsPbIBr_2$ perovskite thin films were fabricated via a solution process. The morphological and structural properties of $CsPbIBr_2$ perovskite thin films prepared under different spin-coating parameters are systematically investigated using SEM, XRD, XPS and EDS. The $CsPbIBr_2$ thin film with 2000 rpm and 120 s exhibits the good crystallinity and large average grain size. Consequently, the optimal rotation speed and time under the experimental conditions are determined to be 2000 rpm and 120 s, respectively. This work provides a novel approach for preparing high-quality $CsPbIBr_2$ perovskite thin films.

(Received September 17, 2025; accepted June 2, 2026)

Keywords: $CsPbIBr_2$ perovskite thin film, Crystallinity, Average grain size

1. Introduction

Today, renewable energy technology is developing rapidly. Among various photovoltaic devices, silicon-based solar cells have achieved commercial application. However, their high manufacturing costs, complex fabrication processes, and photoelectric conversion efficiency (PCE) approaching the theoretical limit pose significant challenges for further breakthroughs. In 2009, a perovskite material ($CH_3NH_3PbI_3$) was applied in dye-sensitized solar cells, achieving an efficiency of 3.8% [1]. Subsequently, there has been an increasing amount of research on perovskite solar cells (PSCs). Over the past decade, the certified efficiency of PSCs with organic components has surpassed 26.7% [2]. Their exceptional optoelectronic properties stem from long carrier diffusion lengths and tunable bandgaps [3,4]. Nevertheless, the presence of volatile organic components in hybrid perovskites leads to material decomposition under high temperature and humidity, severely compromising the long-term stability of device. This has motivated researches toward all-inorganic perovskites ($CsPbX_3$, X=Cl, Br, I). The cesium ions (Cs^+) in $CsPbX_3$ perovskites replace organic cations, significantly enhancing thermal stability [5-8].

Among all-inorganic perovskites, $CsPbI_3$ has received considerable attention owing to its ideal bandgap (~1.7 eV) and high theoretical efficiency [9]. However, it readily undergoes a phase transition at room temperature, which leads to its poor stability. In contrast, $CsPbBr_3$ exhibits excellent phase stability [10,11], but its wide bandgap (~2.3 eV) limits the light absorption range. To balance bandgap and stability, $CsPbIBr_2$ perovskite has emerged [12]. Its bandgap of ~2.1 eV is well-suited for top cells in tandem configurations. Furthermore, the mixed I/Br composition suppresses phase transition, and $CsPbIBr_2$ demonstrates favorable stability [13,14]. Consequently, it is critically important to research $CsPbIBr_2$ perovskite thin films [15]. Currently, the solution spin-coating method is the primary technique for preparing $CsPbIBr_2$ thin films, offering the advantages of simple process and low cost [16]. However, achieving high-quality $CsPbIBr_2$ thin films typically requires glovebox equipment, substantially increasing fabrication costs.

This study employs a solution spin-coating process under ambient air to fabricate $CsPbIBr_2$ perovskite thin films. The influence of various preparation parameters on the morphology and structure of the $CsPbIBr_2$ thin films is systematically investigated using the characterization techniques of SEM, XRD, XPS and EDS.

2. Experimental methods

2.1. Fabrication of $CsPbIBr_2$ perovskites

Fluorine-doped tin oxide (FTO) glasses were treated. All procedures for $CsPbIBr_2$ perovskite thin film preparation were conducted under ambient atmosphere. A

precursor solution was prepared by dissolving 260 mg CsI powder (99.999%) and 367 mg $PbBr_2$ powder (99.999%) in 1 ml dimethyl sulfoxide (DMSO, 99.9%). The precursor solution was stirred for 12 hours to completely dissolve the solution. Subsequently, the precursor solution was dripped onto the FTO substrate, followed by immediate spin-coating. The spin-coating rotation speeds were set to 1500 rpm, 2000 rpm and 2500 rpm, respectively. Meanwhile, the spin-coating times were set to 60 s, 120 s and 180 s, separately. This process yielded as-deposited $CsPbIBr_2$ thin films. Finally, the $CsPbIBr_2$ thin films were heated at 160 °C for 20 min, forming crystalline $CsPbIBr_2$ thin films.

2.2. Characterizations

The surface morphology and grain size of $CsPbIBr_2$ sample were achieved through Scanning Electron Microscopy (SEM). The crystallinity of $CsPbIBr_2$ sample was obtained through X-ray Diffraction (XRD). The element composition of $CsPbIBr_2$ sample was acquired via X-ray Photoelectron Spectroscopy (XPS) and Energy-Dispersive Spectroscopy (EDS).

3. Results and discussions

3.1. Morphological study

Fig. 1 presents the SEM images of $CsPbIBr_2$ perovskite thin films deposited at different spin-coating rotation speeds and times. The $CsPbIBr_2$ perovskite thin film spin-coated at 1500 rpm exhibits irregularly shaped holes (Fig. 1a).

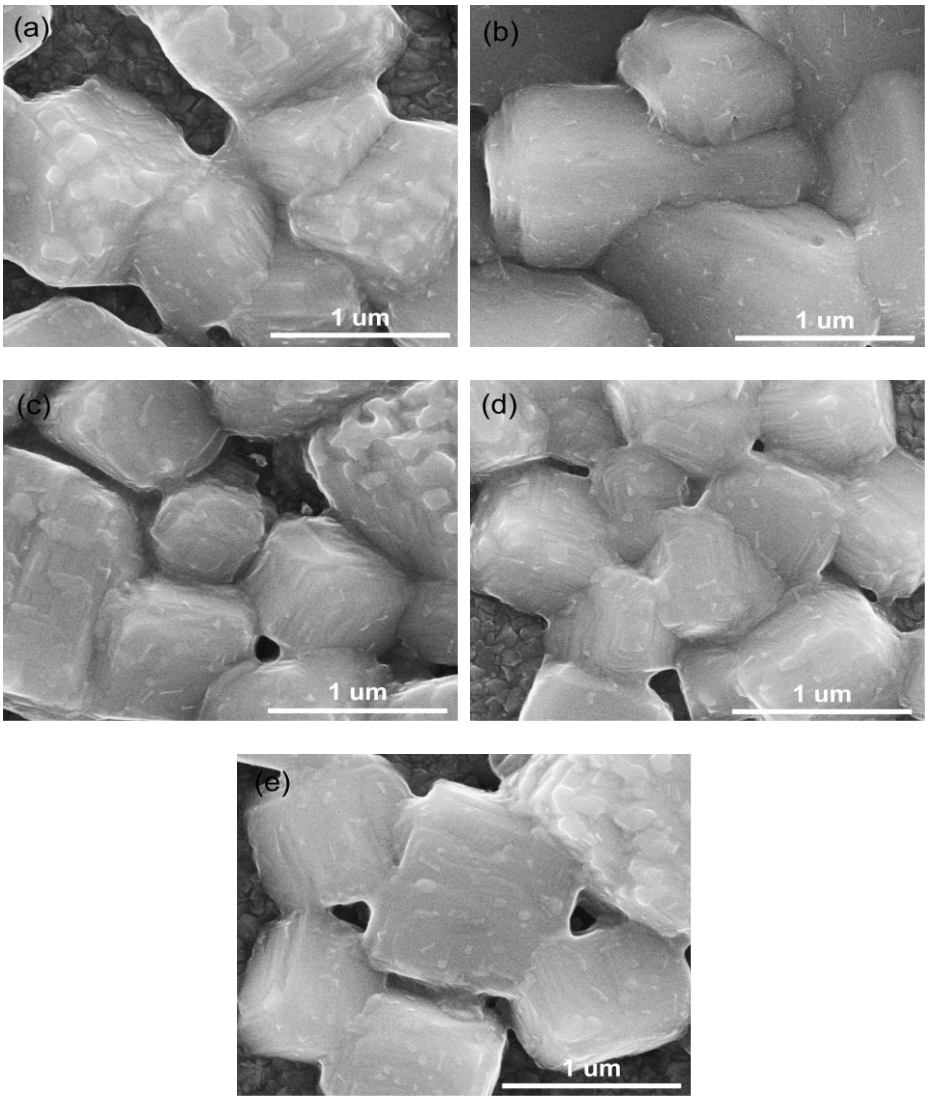

Fig. 1. SEM images of $CsPbIBr_2$ perovskite thin films deposited under various spin-coating parameters: (a) rotation speed of 1500 rpm and time of 120 s; (b) rotation speed of 2000 rpm and time of 120 s; (c) rotation speed of 2500 rpm and time of 120 s; (d) rotation speed of 2000 rpm and time of 60 s; (e) rotation speed of 2000 rpm and time of 180 s

Increasing the rotation speed to 2000 rpm can result in significantly denser films without observable holes (Fig. 1b). However, when the rotation speed is further increased to 2500 rpm, a small number of irregular holes exist (Fig. 1c). The presence of holes typically affects the crystallinity of $CsPbIBr_2$ thin film [17]. Consequently, the thin film deposited at 2000 rpm demonstrates the best crystallinity. To further optimize the fabrication parameters, the effect of spin-coating time on the morphology of $CsPbIBr_2$ thin film is investigated at the optimized rotation speed of 2000 rpm. The $CsPbIBr_2$ thin film prepared at spin-coating time of 60 s displays a small number of holes (Fig. 1d). When the time extends to 120 s, the thin film with better compactness can be obtained (Fig. 1b). However, the holes appear again as the time increases to 180 s (Fig. 1e). Therefore, the $CsPbIBr_2$ thin film with the optimal surface morphology is prepared when the rotation speed reaches 2000 rpm and the time reaches 120 s.

Fig. 2 is the average grain size histograms for $CsPbIBr_2$ perovskite thin films deposited under various parameters. Because the grain shape in Fig. 1 is not completely regular, multiple measurements are made in different areas of each grain to obtain more accurate average grain sizes.

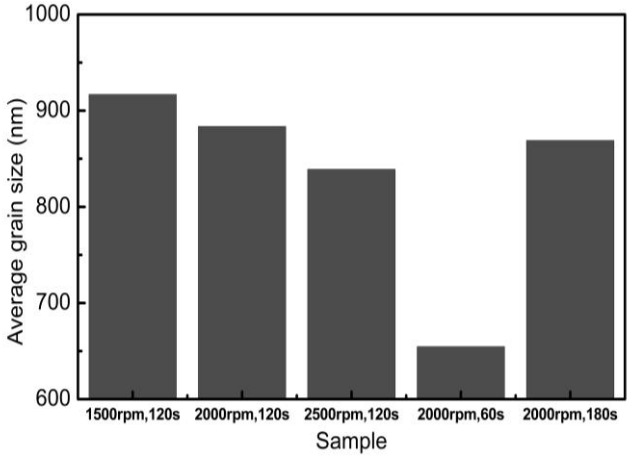

Fig. 2. Average grain size histograms of $CsPbIBr_2$ perovskite thin films deposited under various parameters

As shown in Fig. 2, the average grain size of $CsPbIBr_2$ thin film is 916.89 nm when the rotation speed is 1500 rpm. When the rotation speed increases to 2000rpm, the average grain size of $CsPbIBr_2$ thin film decreases to 883.67 nm. As the rotation speed further increases to 2500 rpm, the average grain size of $CsPbIBr_2$ thin film decreases to 839.08 nm. Consequently, $CsPbIBr_2$ thin film deposited at 1500 rpm exhibits the largest average grain size. Although this condition yields the largest grains, the presence of holes (Fig. 1a) reduces the crystallinity of the thin film [18]. Therefore, the thin film prepared at 2000 rpm shows relatively large grain size. Following the determination of the optimal rotation speed (2000 rpm), the influence of spin-coating time on grain size is investigated. When the time reaches 60 s, the average grain size of $CsPbIBr_2$ thin film is 654.74 nm. When the time improves to 120 s, the average grain size of $CsPbIBr_2$ thin film enhances to 883.67 nm. As the time further boosts to 180 s, the average grain size of $CsPbIBr_2$ thin film decreases to 868.99 nm. Therefore, when the rotation speed and time reach 2000rpm and 120s respectively, the average grain size of $CsPbIBr_2$ thin film is relatively large.

3.2. Structural study

Fig. 3a presents the XRD patterns of $CsPbIBr_2$ perovskite thin films deposited under various parameters. There are two distinct diffraction peaks at 21.68° and 30.59°, which is attributed to the (110) and (200) crystallographic planes [18], respectively. The two peaks observed at 26.95° and 38.21° originate from the FTO substrate [19]. Notably, the intensities of the (110) and (200) peaks are different in the samples, indicating the preferred orientation growth in the $CsPbIBr_2$ thin films. As the spin-coating time increases from 60 s to 120 s, the intensity of the (200) peak enhances, signifying the enhanced crystallinity of the $CsPbIBr_2$ thin films [20]. when the time further increases to 180 s, the intensity of the (200) peak decreases, implying a decrease in crystallinity. Consequently, the $CsPbIBr_2$ thin film with a time of 120 s exhibits the strongest crystallinity. Fig. 3b displays the full width at half maximum (FWHM) values of the (200) diffraction peaks for the $CsPbIBr_2$ thin films deposited under various parameters. As the time increases from 60 s to 120 s, the FWHM of the (200) peak decreases, indicating an enhancement in the average grain size of the $CsPbIBr_2$ thin film. However, prolonging the time to 180 s results in an increase in the FWHM, signifying a reduction in the average grain size.

Therefore, the $CsPbIBr_2$ thin film prepared at the time of 120 s demonstrates the largest average grain size. This aligns with the observations from the SEM.

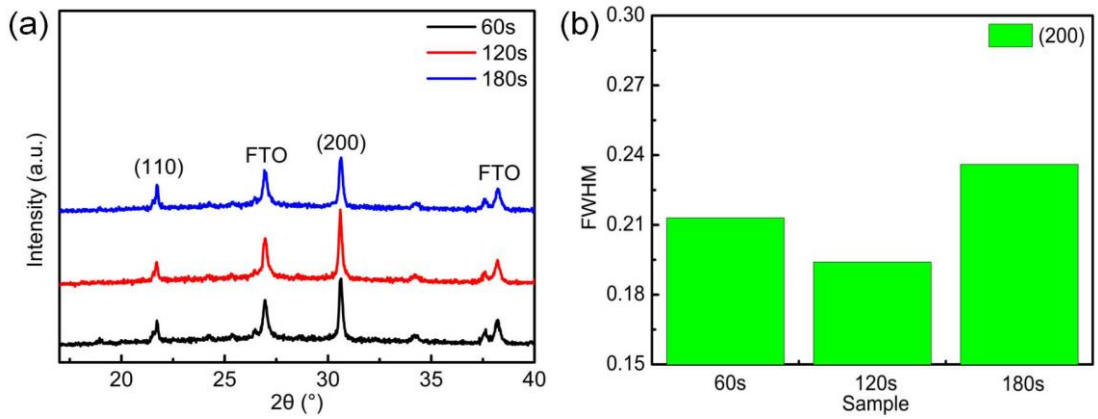

Fig. 3. (a) XRD patterns and (b) FWHM values of the (200) diffraction peak for $CsPbIBr_2$ thin films deposited under various parameters (colour online)

Fig. 4a-4d show the Br 3d, I 3d, Pb 4f and Cs 3d spectra of $CsPbIBr_2$ thin films at the speed of 2000 rpm and the time of 120 s, respectively. $CsPbIBr_2$ thin film contains Br, I, Pb and Cs elements, indicating that $CsPbIBr_2$ thin film has been successfully prepared [21]. Fig. 5 reveals the EDS spectrum of $CsPbIBr_2$ thin film at the speed of 2000 rpm and the time of 120 s. It can be seen from Fig. 5 that there are characteristic peaks of Br, I, Pb and Cs in $CsPbIBr_2$ thin film, showing that there are Br, I, Pb and Cs elements in the thin film, which is supported by the test results in Fig. 4.

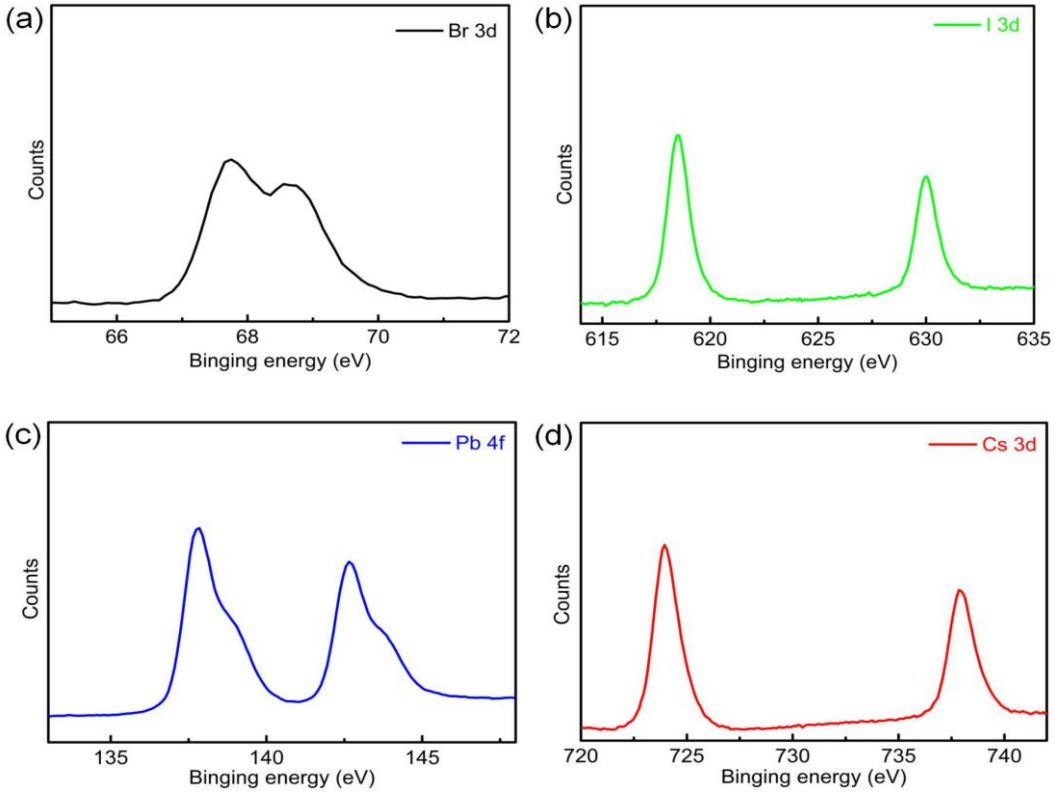

Fig. 4. XPS spectra of the $CsPbIBr_2$ perovskite thin film fabricated at a rotation speed of 2000 rpm and a time of 120 s: (a) Br 3d, (b) I 3d, (c) Pb 4f, (d) Cs 3d (colour online)

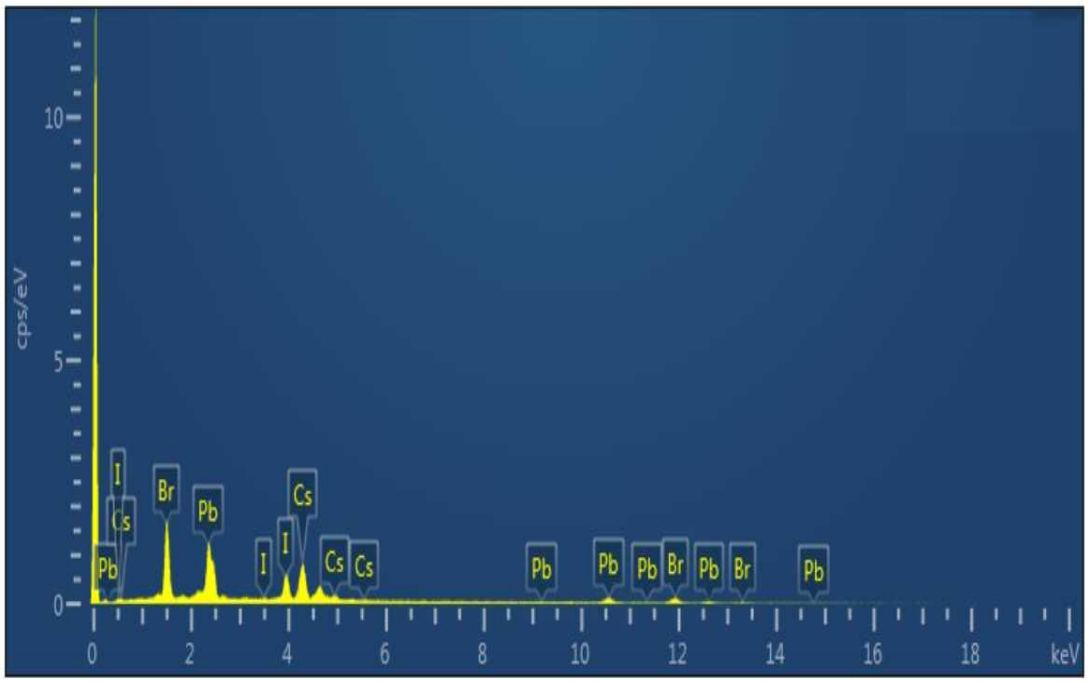

Fig. 5. EDS spectrum of the $CsPbIBr_2$ perovskite thin film fabricated at a rotation speed of 2000 rpm and a time of 120 s (colour online)

4. Conclusions

In this work, $CsPbIBr_2$ perovskite thin films were fabricated via a solution spin-coating method. The effects of spin-coating rotation speed and spin-coating time on the morphology and structure of the $CsPbIBr_2$ thin films are studied. The SEM and XRD tests reveal that the rotation speed and time significantly affect the crystallinity and average grain size of the $CsPbIBr_2$ thin films. The good crystallinity of the $CsPbIBr_2$ thin film is achieved at a rotation speed of 2000 rpm and a time of 120 s. Furthermore, the $CsPbIBr_2$ thin film exhibits large average grain size under these conditions. The XPS and EDS tests confirm the presence of Cs, Pb, I, and Br elements in the $CsPbIBr_2$ thin film, thereby showing the successful fabrication of the $CsPbIBr_2$ thin film.

Acknowledgements

This work was financed by the Changzhou Scientific and Technological Program grant (Grant No. CJ20250087), the National Natural Science Foundation of China (Grant No. 12304043), Project for Building a Science and Technology Innovation Center Facing South Asia and Southeast Asia (Grant No. 202403AP140015), the Key Applied Basic Research Program of Yunnan Province (Grant No. 202201AS070023) and Yunnan Revitalization Talent Support Program, the Spring City Plan: The High-level Talent Promotion and Training Project of Kunming (Grant No. 2022SCP005).

References

[1] J. Chen, Z. Wu, S. Chen, W. Zhao, Y. Zhang, W. Ye, R. Yang, L. Gong, Z. Peng, J. Chen, Materials Science in Semiconductor Processing **174**, 108186 (2024).
[2] Y. Xu, C. Yan, H. Liang, S. Huang, P. Feng, J. Song, Nanotechnology **35**, 175404 (2024).
[3] K. Chen, P. Wu, W. Yang, R. Su, D. Luo, X. Yang, Y. Tu, R. Zhu, Q. Gong, Nano Energy **49**, 411 (2018).
[4] Y. Guo, J. Jiang, S. Zuo, F. Shi, J. Tao, Z. Hu, X. Hu, G. Hu, P. Yang, J. Chu, Solar Energy Materials and Solar Cells **178**, 186 (2018).
[5] H. Yuan, Y. Zhao, J. Duan, B. He, Z. Jiao, Q. Tang, Electrochimica Acta **279**, 84 (2018).
[6] G. Liao, J. Duan, Y. Zhao, Q. Tang, Solar Energy **171**, 279 (2018).
[7] F. Zhao, Y. Guo, P. Yang, J. Tao, J. Jiang, J. Chu, Journal of Alloys and Compounds **930**, 167377 (2023).
[8] F. Zhao, Y. Guo, P. Yang, J. Chu, J. Optoelectron. Adv. M. **27**(5-6), 255 (2025).
[9] P. Luo, Y. Zhou, S. Zhou, Y. Lu, C. Xu, W. Xia, L. Sun, Chemical Engineering Journal **343**, 146 (2018).

[10] J. Lei, F. Gao, H. Wang, J. Li, J. Jiang, X. Wu, R. Gao, Z. Yang, S. Liu, Solar Energy Materials and Solar Cells **187**, 1 (2018).
[11] P. Teng, X. Han, J. Li, Y. Xu, L. Kang, Y. Wang, Y. Yang, T. Yu, ACS Applied Materials and Interfaces **10**, 9541 (2018).
[12] X. Tan, X. Liu, Z. Liu, B. Sun, J. Li, S. Xi, T. Shi, Z. Tang, G. Liao, Applied Surface Science **499**, 143990 (2020).
[13] W. Zhang, J. Xiong, J. Li, W. A. Daoud, Small **16**, 2001535 (2020).
[14] W. Zhu, Q. Zhang, D. Chen, Z. Zhang, Z. Lin, J. Chang, J. Zhang, C. Zhang, Y. Hao, Advanced Energy Materials **8**, 1802080 (2018).
[15] Y. Long, C. Wang, X. Liu, J. Wang, S. Fu, J. Zhang, Z. Hu, Y. Zhu, Journal of Materials Chemistry C **9**, 2145 (2021).
[16] Y. Guo, F. Zhao, X. Wang, J. Tao, D. Zheng, J. Jiang, Z. Hu, J. Chu, Solar Energy Materials and Solar Cells **221**, 110918 (2021).
[17] J. Duan, Y. Zhao, X. Yang, Y. Wang, B. He, Q. Tang, Advanced Energy Materials **8**, 1802346 (2018).
[18] Y. Zhao, Y. Wang, J. Duan, X. Yang, Q. Tang, Journal of Materials Chemistry A **7**, 6877 (2019).
[19] F. Zhao, Y. Guo, J. Tao, Z. Li, J. Jiang, J. Chu, Applied Optics **59**, 5481 (2020).
[20] F. Zhao, Y. Guo, Q. Yang, P. Yang, J. Chu, Optoelectron. Adv. Mat. **19**(3-4), 202 (2025).
[21] Y. Guo, F. Zhao, Z. Li, J. Tao, D. Zheng, J. Jiang, J. Chu, Organic Electronics **83**, 105731 (2020).

*Corresponding authors: fzhaobs@126.com; yxguo@shnu.edu.cn